Screening of Coulombic Interactions to Achieve Higher Power Factor in Conjugated Polymers

Pawan Kumar[1 $ *], Anas Abutaha[3 $], Gang Wu[2 $], Madeleine P. Gordon[4,5], Jose Recatala-Gomez[6], Jeffrey J. Urban[4], Kedar Hippalgaonkar[1 6 *]

[1] Institute of Materials Research and Engineering, Agency for Science Technology and Research, #08-03, 2 Fusionopolis Way, Innovis, Singapore 138634

[2] Institute of High Performance Computing, Agency for Science Technology and Research, 1 Fusionopolis Way,#16-16 Connexis (North Tower) Singapore 138632

[3] Qatar Environment and Energy Research Institute (QEERI), Hamad Bin Khalifa University (HBKU), P.O. Box 34110, Doha, Qatar

[4] Molecular Foundry, Lawrence Berkeley National Laboratory, 1 Cyclotron Road, Berkeley, CA, 94720 USA.

[5] Applied Science and Technology Graduate Group, University of California, Berkeley, CA, 94720, USA.

[6] School of Materials Research and Engineering, Nanyang Technological University, Block N4.1 , 50 Nanyang Avenue, Singapore 639798

$ Authors contributed equally.

*-Corresponding authors.

Correspondence to: pawankumar@imre.a-star.edu.sg and kedar@ntu.edu.sg

Keywords: Organic thermoelectric, dielectric constant, doping, power factor, conducting polymer, thin film.

Abstract

Thermoelectric properties of conducting polymers typically suffer from molecular chain disordering as charge transport is predominantly controlled by morphology. This is especially more problematic when counter-ions are introduced to tune the carrier concentration for optimal thermoelectric performance, which disturbs the morphology further. In this work, we introduce a new avenue for enhancing thermoelectric properties without needing to regulate the morphology, namely by controlling the coulombic interaction between polarons and counterions. We perform insitu de-doping thermoelectric experiments over 3 orders of magnitude change in electrical

conductivity of three distinct thermoelectric polymers, namely poly(3-hexylthiophene-2,5-diyl) (P3HT), Poly[2,5-bis(3-dodecylthiophen-2-yl)thieno[3,2-b]thiophene] (PBTTT-C_{12}) and Poly[2,5-(2-octyldodecyl)-3,6-diketopyrrolopyrrole-alt-5,5-(2,5-di(thien-2-yl)thieno [3,2-b]thiophene)] (OD-PDPP2T-TT) conjugated polymers, followed by Grazing Incidence Wide Angle X-ray Scattering (GIWAXS) to study their respective morphologies. We demonstrate a nine-fold enhancement in the thermoelectric power factor in OD-PDPP2T-TT compared to PBTTT-C_{12} and link it to the coulombic screening of charge carriers, including in the optimally doped regime. We support this hypothesis by using Boltzmann transport equations, and show that in both P3HT and PBTTT-C_{12} as the polymer is doped, impurity scattering remains the dominant scattering mechanism, while in OD-PDPP2T-TT, the scattering mechanism changes from impurity to acoustic-phonon limited resulting in more effective screening of ionized counterions. Our results provide an additional knob to enhance the fundamental understanding of thermoelectric physics of conducting polymers, and provide a pathway to achieving higher performance in the field of organic thermoelectrics.

Introduction:

A large part (~66 %) of waste heat due to industrial processes is released below 200°C[1], and thermoelectric devices possess considerable potential for converting it into useful electrical power. The efficiency of a thermoelectric material depends on the figure of merit, $ZT = \frac{S^2\sigma T}{\kappa}$ where S is the Seebeck coefficient, σ is electrical conductivity, κ is total thermal conductivity, and T is the thermodynamic temperature. Although inorganic materials, the commercially available industry standard, have shown good thermoelectric properties over a wide range of operation temperatures, they are expensive and potentially toxic, which ultimately limits their widespread deployability[2, 3]. On the other hand, conducting polymers are good contenders for near room temperature applications due to their solution processability and earth abundance. Recently, poly- (ethylenedioxythiophene) (PEDOT) based polymers have shown promising thermoelectric properties at room temperarure either by controlling the morphology or the dopant volume[4, 5, 6]. Along with PEDOT, poly(3-hexylthiophene) (P3HT) and poly(2,5-bis(3-alkylthiophen-2-yl) thieno[3,2-b]thiophene) (PBTTT) have also shown promising thermoelectric (TE) properties at room temperature by modifying their structural morphology[7, 8] and controlling the doping process to avoid further structrural disorder due to fluctuation in the inter-chain spacing known as paracrystallinity[9-13]. The dopants introduce polarons within the polymer backbone, which provide itinerant charge carriers resulting in electrical transport. However, with the introduction of polarons via such externally added dopant molecules, morphological changes and increased disorder can result, depending on their size and distribution. These disruptions can be detrimental to conductivity [7, 13, 14, 15, 16], and arise from the distortion due to ionized counterions in the polymer matrix. In addition, a strong Coulombic interaction between ionized counterions and polarons effectively hinders the charge mobility of polarons further. Aubry et. al.[17] have controlled the

separation between counterions and polarons by choosing dodecaborane (DDB) based dopants that act to reduce the Coulombic interaction between them and hence improve the conductivity of the P3HT polymer film. But, due to the large size of the DDB-F_{72} dopant, morphological disorder is increased, which adversely impacts the charge mobility. Therefore, we hypothesize that reducing the Coulombic interaction between counterions and delocalized polarons without disturbing the morphology will be the key to further enhance the TE properties in conducting polymers. This can effectively be done either by controlling the dielectric environment or distance between the polarons and counterions.

The effect of dielectric constant on photovolatic properties of organic polymers has been well studied[18]. Namchul cho et. al.[19] have shown that by incorporating polar nitrile side-chains in diketopyrrolopyrrole indacenodithiophene polymer (DPP-IDT-CN) compared to an analogous polymer with alkyl side-chains (PIDT-DPP-Alkyl), the dielectric constant of the donor material increases from 3.9 to 5. This increase results in longer carrier lifetimes, improving both the open-circuit voltage and short-circuit current in DPP-IDT-CN /C60 bulk heterojunction (BHJ) photovoltaic devices. Jeroen Brebels et. al.[20] have shown that by replacing alkyl side chains with oligo(ethylene glycol) side chains in poly[2,6-(4,4′-dihexyl-4H-cyclopenta[2,1-b;3,4-b′]dithiophene-alt-N-alkylthieno[3,4-c]pyrrole-4,6-dione (PCPDT-TPD) co-polymer, dielectric constant changes from 3.1 to 6.3. Wang et.al., have shown a remarkable enhancement in dielectric constant in P3HT by adding sulfinyl and sulfonyl groups within the alkyl side chains[21]. The dielectric constant at room temperature was shown to increase from 3.75 for P3HT to 7.4 for the sulfinylated and 8.1–9.3 for sulfonylated P3HT polymers. However, while side chain modification is a powerful approach for improving the dielectric constant in P3HT, it often disrupts packing morphology, and increases the distance between the π-π stacks, both of which are not beneficial

for charge transport[22 23]. Alternatively, diketopyrrolopyrrole (DPP)-based low bandgap poly[2,5-(2-decyltetra-decyl)-3,6-diketopyrrolopyrrole-alt-5,5-(2,5-di(thien-2-yl)thieno [3,2-b]thiophene)] (DT-PDPP2T-TT) co-polymer has also shown a higher dielectric constant without side chain modification[24].

In this work, we therefore show that the dielectric constant of the polymer matrix itself can be used to boost TE properties without causing major morphology disruptions at various levels of doping. Here, we reveal the connection between dielectric constant and thermoelectric transport properties of *p*-doped P3HT, PBTTT and poly[2,5-(2-octyldodecyl)-3,6-diketopyrrolopyrrole-alt-5,5-(2,5-di(thien-2-yl)thieno [3,2-b]thiophene)] (OD-PDPP2T-TT) co-polymers. P3HT and PBTTT-C_{12} are well known *p*-type semi-crystalline polymers[25 26]. OD-PDPP2T-TT, which is a donor-acceptor (D-A) co-polymer has also shown *p*-type nature with similar degrees of semi-crystallinity[27]. We measure the thermoelectric power factor ($PF = S^2\sigma$) and compare the effect of the degree of disorder in these conducting polymers. We have measured an optimum PF of 66 $\mu Wm^{-1} K^{-2}$ for OD-PDPP2T-TT, which is >8x times larger than PBTTT, which has a PF=7.8 $\mu Wm^{-1} K^{-2}$ and >40x higher than P3HT, which shows PF = 1.6 $\mu Wm^{-1} K^{-2}$ with similar or higher structural disorder described by their paracrystallinity[12]. The Seebeck coefficient depends only on the carrier concentration (n)(for fix effective density of state mass), while the conductivity (σ) depends on both carrier concentration (n) and the carrier mobility (μ). Hence, by increasing the dielectric constant to aid screening of the polarons in OD-PDPP2T-TT, their Coulombic interaction with the externally introduced counterions can be reduced, thus enhancing the charge mobility, and resulting in an improved σ.

Results and Discussion:

Firstly, we study the morphology in both pristine and doped films of P3HT, PBTTT-C_{12} and OD-PDPP2T-TT polymers, by performing GIWAX and GIXRD for both pristine and doped films, as shown in Figure 1(a-f). All films were doped by a 0.03 M concentration of $FeCl_3$. For P3HT, out-of-plane (h00) scattering peaks up to the third order, are attributed to the lamellar structure, as well as an inter-chain (010) peak attributed to π–π stacking, are observed, indicating a semi-crystalline nature with preferential edge-on orientation[10]. For PBTTT(Fig 1(c-d)), peaks indicative of lamellar structure up to the fourth order in the out-of-plane direction, as well as an inter-chain peak were observed, revealing an edge-on orientation with even better chain alignment than P3HT, as has been previously reported in literature[28]. In the case of OD-PDPP2T-TT(Fig 1(e-f)), while lamellar peaks are observed in out-of-plane direction, the inter-chain peak is prominent in the in-plane direction, suggesting that PDPP2T-TT thin films are edge-on oriented with respect to the SiO_2 substrate.. For pristine P3HT, the (100) and (010) distances were found to be 15.85 and 3.80 Å, respectively, which are close to values reported in literature[10]. After doping, P3HT films retain their edge-on orientation and no appreciable shift in (010) peak location is seen, as shown in Fig. 1(a-b), suggesting that the counterions do not change the π–π stacking of the film further. In the case of pristine PBTTT, lamellar and π–π stacking distances were found to be 20.65 and 3.678Å, respectively, which are consistent with reported values[29]. After doping, the peak positions shifted to 21.43 and 3.61Å and edge-on orientation was maintained. The small shift in lamellar and π–π stacking distances shows marginal variation in structural disorder of the PBTTT with $FeCl_3$ doping. The shift in lamellar distance indicates that the counterions are intercalated between the alkyl side chains, and concurrently reduce the π–π stacking distance, which in turn strengthens the π–π orbital overlap, hence improving the delocalization of charge carriers[10 30]. For OD-PDPP2T-TT, the lamellar and π–π stacking distances were observed to be 19.3 and 3.87 Å, respectively,

which are comparable to those published previously[27]. After doping, lamellar distance increases and reaches 23.2 Å, while no change is observed in the π–π stacking distances and it stays at 3.92 Å.

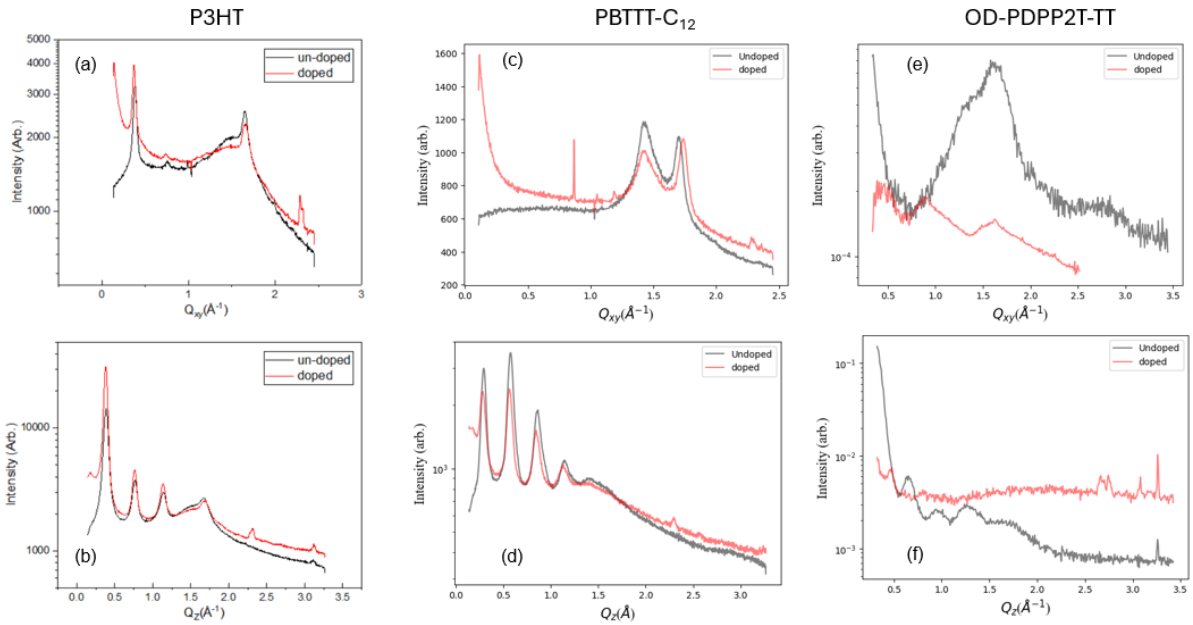

Fig. 1: **GIWAX data of undoped and doped P3HT, PBTTT-C12 and GIXRD OD-PDPP2T_TT polymer films on SiO2 substrate** (a-f). 2D diffractograms of the P3HT, PBTTT and OD-PDPP2T-TT thin films on SiO_2 substrate before (black) and after doping (red) of P3HT, PBTTT and OD-PDPP2T-TT thin films.

Structural disorder is generally described by paracrystallinity (g), which represents the fluctuation in the π–π stacking spacing distance. A general relationship between charge transport and paracrystallinity in conducting polymers is known[12], where higher g is known to produce more localized states in a material's electronic band gap, which limits charge transport [12]. Here, paracrystallinity [$g_{(010)}$] can be derived from $g^2_{(010)} = \langle(\delta/d_0)^2\rangle = \langle d^2\rangle/d_0^2 - 1$, where d is the π-π stacking distance observed from the radial intensity plots from Figure 1(b), and $d_0 = \langle d\rangle$ is the averaged π-π stacking distance along (010) direction, while $\delta = d - d_0$ represents the change of π-π stacking distance between the adjacent polymer chains in that specific crystal direction of

[010]. In reciprocal space, g can be written as: $g_{(010)} = \sqrt{\frac{\Delta q}{2\pi q_0}}$, where (q_0) is the peak position, and Δq is the FWHM of the scattering peak[12 18] along the π–π stacking direction in GIWAXS measurement. π-π stacking distance was chosen because it is the predominant direction for charge transport. As shown in Table 1, the pristine PBTTT film possesses a lower g compared to P3HT, indicating that PBTTT chains tend to be more aligned under the same processing conditions. On the other hand, OD-PDPP2T-TT film exhibit the highest g value compared to P3HT and PBTTT films. After doping, structural disorder was less affected in P3HT and OD-PDPP2T-TT films by $FeCl_3$ doping, but an appreciable effect was observed in PBTTT films as the g value increases from 6.6 to 8%.

Material	q_0 (Å^{-1})	Δq (Å^{-1})	$g_{(010)} = \sqrt{\frac{\Delta q}{2\pi q_0}}$
P3HT (undoped)	1.6533	0.0737	8.4 %
P3HT (doped)	1.657	0.07908	8.7 %
PBTTT (undoped)	1.705	0.0471	6.6 %
PBTTT (doped)	1.7402	0.07018	8.0 %
OD-PDPP2T-TT (undoped)	1.62	0.2	13.8 %
OD-PDPP2T-TT (doped)	1.615	0.22	14.1 %

Table 1. Paracrystallinity change from pristine to doped P3HT, PBTTT and OD-PDPP2T-TT polymer thin films.

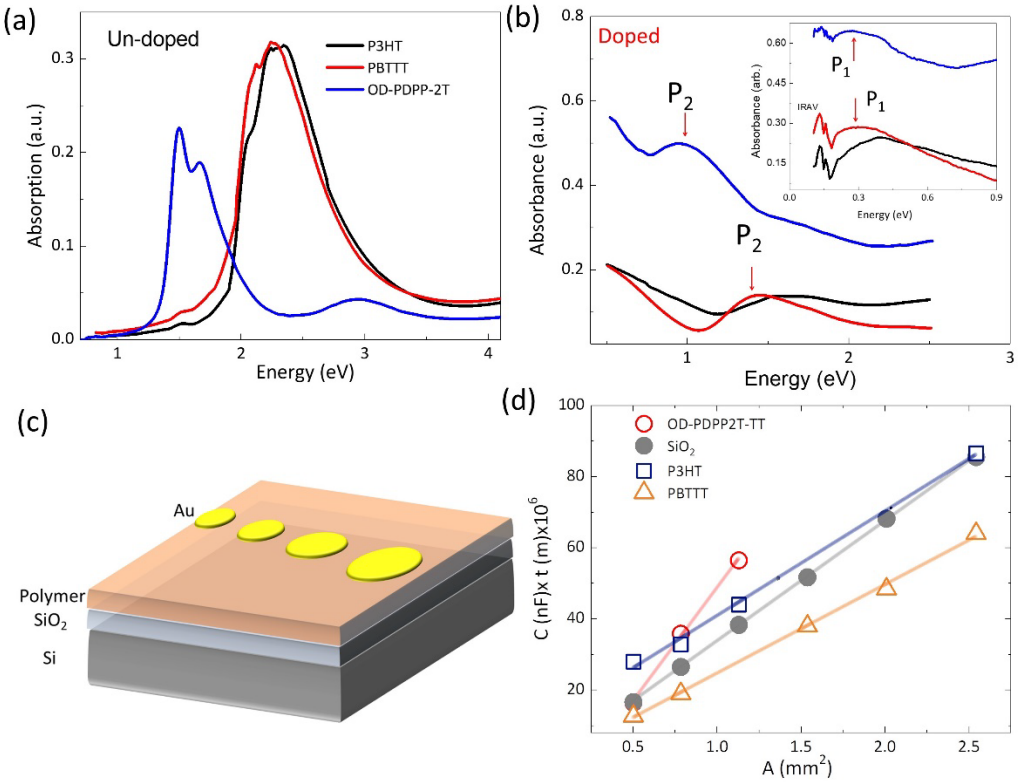

Fig. 2: **UV-Vis spectra and dielectric measurement of P3HT, PBTTT-C_{14} and OD-PDPP2T-TT polymers** (a) UV-Vis spectra of the pristine and (b) Doped P3HT, PBTTT-C_{14} and OD-PDPP2T-TT polymer thin films with 0.03M concentration of $FeCl_3$. Inset of figure (b) shows FTIR spectra of doped samples. (c) Schematic of the measurement geometry and the dielectric constant of different conjugated polymer films. (d) Capacitance (C) × thickness (t) of polymer thin films as a function of area (A) for un-doped P3HT (blue squares), PBTTT (orange triangles) and OD-PDPP2T-TT (red circles) and SiO_2 (grey circles). Thin films of P3HT, PBTTT-C_{12} and OD-PDPP2T-TT polymer were prepared by spin coating in di-chlorobenzene solution.

While GIWAXS provides information about the structural morphology of the polymer chains, we next perform ultraviolet-visible (UV-Vis) light absorption studies on the pristine and doped P3HT, PBTTT and OD-PDPP2T-TT films to understand the extent of delocalization of the polarons. The spectra of P3HT thin films in Figure 2(a) shows a dominant peak at E = 2.36 eV corresponding to an intra-chain π -π* transition, with two small shoulders at energies 2.23 and 2.06 eV corresponding to inter-chain π –π stacking interactions and high planarity[31 32]. The UV-Vis spectra of PBTTT thin films depict a main absorption peak around 2.24 eV followed by a weak

shoulder around 2.12 eV which are linked to intra-chain and inter-chain π -π* transitions respectively[11 33]. The intensity of the weak shoulder in PBTTT is stronger compared to P3HT which is a manifestation of high crystallinity and more backbone planarity in the PBTTT thin film, as confirmed by the GIWAXS analysis. On the other hand, UV-Vis spectra of OD-PDPP2T-TT thin films shows a strong absorption below 2 eV. Two peaks in absorption were observed around 1.66 and 1.50 eV, which are consistent with reported spectra for OD-PDPP2T-TT[27] .

Next, Figure 2(b) shows the absorption spectra of the doped films. The data is shown until 0.5 eV due to the limitation of UV-vis-NIR spectrometer. The P_2 peak is clearly visible in the UV-Vis-NIR spectra for all polymers. FTIR measurements were performed below 0.5 eV to observe P_1 peak as shown in Fig. 2(b) inset. P_1 and P_2 absorption for P3HT is observed around 0.38 eV and 1.55 eV which are close to those reported in literature32. In the doped PBTTT film, the P_2 peak is observed around 1. 45 eV and P_1 peak is found around 0.32 eV similar to those reported for PBTTT doped with $FeCl_3$ previously [34]. A red shift in the P_1 position in PBTTT, as compared to P3HT, is a signature of more delocalized carriers linked to its high crystallinity[16, 33]. In the case of OD-PDPP2T-TT, the P_2 peak is observed around 1 eV and P_1 peak was found around 0.27 eV. A red shift in P_1 for OD-PDPP2T-TT suggests that the carriers are even more delocalized compared to PBTTT. On the other hand, OD-PDPP2T-TT shows a relatively higher paracrystallinity (see Table 1). Therefore, higher crystallinity can't be the reason for the red shift in the OD-PDPP2T-TT polymer thin film. An alternate factor that controls the carrier delocalization is the Coulombic interaction between polarons and the counterions. For example, it has shown that by choosing a larger size of dopant molecule, the average distance between polaron and counter-ion can be increased, which decreases the Coulombic interaction between polarons and counterions giving rise to higher conductivity[32 35 36]. In our case, the same dopant, namely,

$FeCl_3$ was used. Therefore, we postulate that the dielectric environment of the polymer matrix must tune this Coulombic interaction.

To support this hypothesis, we measure the static dielectric constant of all three polymers. For this, we devise a cross-plane configuration, as shown in the upper panel in Figure 2(c), where the polymer film (on SiO_2) is sandwiched in between patterned metal discs of different areas on the top and the highly conducting doped silicon substrate at the bottom. The capacitance (C) multiplied by the thickness (t) of each polymer thin film as a function of area (A) for P3HT, PBTTT-C_{12} and OD-PDPP2T-TT respectively, are plotted in Figure 2(d). The capacitance of SiO_2 as a function of area was measured as a reference, without any polymer films. The slope of $C \times t$ versus A represents the dielectric constant of the polymer (See SI for more details about the chosen axis). The value of the static dielectric constant for SiO_2 was found to be 3.2, which is consistent with the reported value in the literature[37]. After measuring the SiO_2 dielectric constant, polymer thin films were spin coated on SiO_2. While the $C \times t$ versus A slope for P3HT and PBTTT looks similar to SiO_2, as evidenced in Fig. 2(d), a higher slope is observed for OD-PDPP2T-TT. The dielectric constant of each polymer was deduced using a series combination of capacitances from the SiO_2 and the polymer (for more details please see methods in SI). The resultant dielectric constant values are shown in Table 2. Higher dielectric constant value for OD-PDPP2T-TT was also supported by DFT calculations (see SI for more details).

	SiO_2	**P3HT**	**PBTTT**	**OD-PDPP2T-TT**
Dielectric constant (ε_s)	3.3	2.8	2.5	6.3

Table 2. Measured static dielectric constant of different polymers, with SiO_2 used as a reference.

Armed with experimentally measured morphology, extent of delocalization and the dielectric constants of the polymers, we measure the thermoelectric transport properties of the

polymer films with the aim to develop a modified charge transport model to fully understand their thermoelectric performance. Figure 3(a) shows the schematic of our vacuum de-doping experiment to generate a large range of Seebeck coefficient versus conductivity data (over 3 orders of magnitude change). All three polymers were first doped with 0.03 M concentration of $FeCl_3$ and de-doping was done under high vacuum (for more details please see methods in SI). In short, under vacuum, the dopants start to escape from the polymer matrix, which causes de-doping. In our previous work[38], we have demonstrated that structural disorder results in a Gaussian tail in the density of states (DOS). Therefore, the total effective DOS can be written as a convolution function of the original DOS and the Gaussian broadening function, given by (for more details see methods in SI):

$$D_v(E) = \frac{1}{\sqrt{\pi}} \int D_v^0 \left((E_v - E) - \sigma_{\text{eff}} \frac{E}{w} \right) e^{-\frac{E^2}{w^2}} dE, \quad (1)$$

where $D_v^0(E)$ is the DOS of the valence band without structural disorder ($g = 0$), w is the Gaussion broadening due to structural disorder, and σ_{eff} is the effective Gaussian broadening due to both screening effect and the structural disorder (see Figure S3 in the Supplementary Information demonstrating the modified 3D DOS with a Gaussian tail, in which the modified DOS around the Fermi level can penetrate the gap region). Using the generalized Boltzmann Transport Equation, the electrical conductivity can then be described as:

$$\sigma = \frac{2q^2}{3m_c^*} \int \tau(E) E D_v(E) \left(-\frac{\partial f}{\partial E} \right) dE, \quad (2)$$

where $\tau(E)$ is relaxation time and can be written as a contribution from acoustic phonons $\tau_{AP}(E)$ and impurity scattering $\tau_{II}(E)$ times, respectively within the Mathieson's rule framework:

$$\frac{1}{\tau(E)} = \frac{1}{\tau_{AP}(E)} + \frac{1}{\tau_{II}(E)} \quad (3)$$

The Seebeck coefficient can be defined as:

$$S = \frac{1}{eT\sigma}\int_0^\infty \sigma_E \left(-\frac{\partial f}{\partial E}\right)(E - E_F)\, dE \tag{4}$$

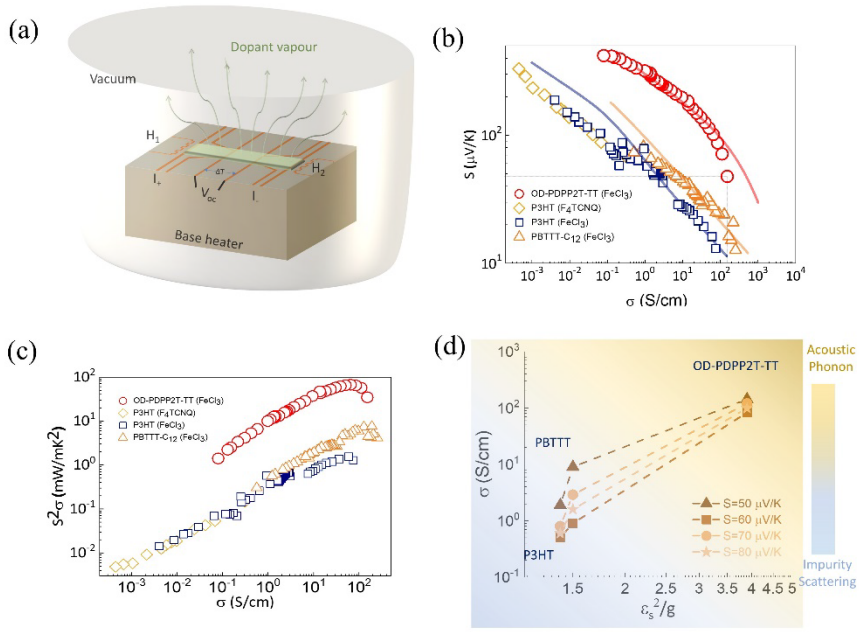

FFigure 3: **Measurement of thermoelectric Power factor ($S^2\sigma$) of dopant- and dielectric-controlled polymers** (a) Vacuum-chamber to de-dope the polymeric thin films under continuous application of vacuum, while the patterned heaters and thin-film thermometers can measure the $S^2\sigma$ *in-situ*. (b) Measured Seebeck coefficient (S) as a function of conductivity (σ) and (c) Power factor as a function of conductivity of P3HT (square), PBTTT (triangle) and OD-PDPP2T-TT (circle) thin films. Charge transport model using effective density of states (more details in SI) was applied on the P3HT, PBTTT and OD-PDPP2T-TT thin films respectively and fits well in the delocalized carrier regime ($\sigma > 1$ S/cm), while it does not capture the localized carrier regime (details in SI). (d) Conductivity as a function of $\frac{\varepsilon_s^2}{g}$, where ε_s is the static dielectric constant of pure polymer matrix without any doping and g is the paracrystallinity. Conductivity values were taken at different Seebeck coefficient values.

Figure 3(b) shows the measured Seebeck coefficient (S) as a function of electrical conductivity (σ) of P3HT, PBTTT-C_{12} and OD-PDPP2T-TT thin films. As expected, S increases as σ decreases with de-doping for all three polymers. This *in-situ* de-doping technique allows us to consider the same value of Seebeck coefficient for all the three polymers, therefore corresponding to the same doping level (horizontal black dashed line in Fig. 3(b)). Here we chose a Seebeck value of 50 μV/K, which is the point at which the power factor peaks for OD-PDPP2T-TT polymer as seen in Figure 3(c). At this value, OD-PDPP2T-TT shows >14x higher conductivity compared to P3HT and PBTTT-C_{12} thin films (vertical dashed line in Fig. 3(b)), which can be attributed to the higher

dielectric constant with strong counterion screening. Solid color lines in Fig. 3(b) show the calculated values from the charge transport model and illustrate that experimental data of *S* versus σ for all three polymers coincides well with our modified charge transport model for a conductivity higher than 1 S/cm, where the modified DOS model is accurate. Interestingly, for P3HT and PBTTT-C_{12} the theoretically modelled solid lines show a near-linear trend in the experimental data, OD-PDPP2T-TT sees a distinct slope change at higher conductivity values (close to 100 S/cm). We hypothesize that this slope change is caused by a change in the scattering of the mobile polarons from impurity to acoustic-phonon limited, which is analogous to metallic transport ($S \propto \frac{1}{\sigma}$) in PBTTT-$C_{12}$ by electrolyte gating as discussed by Tanaka et. al.[29]. Note that below a conductivity of 1 S/cm, we expect Fermi level pinning in localized states due to structural disorder and hence a hopping transport model is more relevant[39 40] than our delocalized charge transport model which is suitable to explain transport at higher doping regimes.

Next, we observe the maximum power factor in our films by plotting the power factor ($S^2\sigma$) as a function of conductivity in Fig. 3(c). The power factor initially increases with conductivity for all polymers until it shows a peak at higher conductivity values and then drops. The optimal power factor value was found to be 1.58 μW/mK^2, 7.8 μW/mK^2 and 66 μW/mK^2 for P3HT, PBTTT and OD-PDPP2T-TT, respectively. A nine-fold enhancement in power factor is therefore observed for OD-PDPP2T-TT, compared to the PBTTT film, without any attempts to alter the morphology. To understand the higher power factor in OD-PDPP2T-TT compared to PBTTT and P3HT better, in Figure 3(d), we plot conductivity as a function of $\frac{\varepsilon_s^2}{g}$ at different Seebeck coefficient values, where ε_s is the static dielectric constant of pure polymer and g is paracrystallinity. Then, we consider the individual contributions to the relaxation times: $\tau_{AP}(E)$ and $\tau_{II}(E)$, which are expected to be proportional to the effective mass of the charge carriers (see

Eq. 10 and 13 in supplementary information for details). For ionized impurity dominated scattering, the mobility of the carriers is proportional to the square of the static dielectric constant (ε_s) and square root of conductivity mass (m_c^*) (See Equation 13 in SI). However, $\tau_{AP}(E)$ does not depend on the static dielectric environment ((See Equation 10 in SI)). Paracrystallinity, g alters the degree of energetic disorder in the electronic structure significantly[12]. This structural disorder broadens the density of states which will increase the effective mass of the carriers. Therefore, g can be correlated with m_c^* of conducting polymers[12]. For a Seebeck value of 75μV/K, which corresponds to a doping level where the charge transport is dominated by impurity scattering, OD-PDPP2T-TT shows one order of magnitude higher conductivity compared to P3HT and PBTTT due to a larger ratio of $\frac{\varepsilon_s^2}{g}$ as shown in Fig. 3(d). A linear trend is observed between conductivity and $\frac{\varepsilon_s^2}{g}$ in this regime. As the Seebeck coefficient drops from 75μV/K to 50 μV/K, the linear trend starts to deviate. This deviation occurs as the scattering mechanism starts to switch from impurity scattering to acoustic phonon limited for OD-PDPP2T-TT; on the other hand, charge transport in both P3HT and PBTTT continues to be dominated by impurity scattering (details in Fig. S4). The deviation increases further as the Seebeck coefficient drops further with increased doping. For the lowest Seebeck coefficient (50 μV/K), the conductivity value for OD-PDPP2T-TT is comparable to that of PBTTT. At this doping level, the dominant scattering mechanism is acoustic phonon scattering in OD-PDPP2T-TT (details in Fig. S4). Here, the effect of the dielectric constant and counterion screening on relaxation times diminishes and only structural order dependence remains (See Equation 0.6 in SI). Therefore, as can be seen in Figure 3(d), the power factor for OD-PDPP2T-TT drops sharply and drops to a value lower than PBTTT at the highest doping level. This is expected as at high doping regimes, PBTTT is more structurally ordered compared to OD-PDPP2T-TT (see Table 1 and Figure 1c). Hence, in the optimal doping range, dielectric constant

of the polymer is a robust metric that determines the counterion screening and therefore controls charge transport towards achieving maximal thermoelectric performance. While we clearly see an enhanced performance due to the dielectric constant providing screening of mobile polarons, this is still far from the maximum potential that can be achieved in conducting polymers.

Conclusion:

In summary, the present study reveals that the thermoelectric power factor in conducting polymers can be further improved by controlling the dielectric constant of the polymer without regulating the structural disorder. A 9-fold enhancement was observed in power factor for OD-PDPP2T-TT compared to PBTTT. The maximum power factor is observed at the crossover point from impurity scattering to acoustic phonon scattering in OD-PDPP2T-TT. By leveraging the higher mobility of charge carriers arising from a higher dielectric constant, we can get large electrical conductivity in these conducting polymers without sacrificing the Seebeck coefficient. Finally, we expect that building on this work, developing new methods to improve the dielectric constant of polymer matrix and further control of morphology will provide a new avenue to augment organic thermoelectric materials.

Materials and methods:

Materials:

Electronic grade P3HT was bought from Rieke metals (weight-average molecular weight Mw ~ 50-70 kg mol−1), PBTTT(-C14) (weight-average molecular weight Mw ~ 40-80 kg mol−1) was purchased from Sigma Aldrich and OD-PDPP2T-TT (weight-average molecular weight Mw ~ 250-300 kg mol−1) was purchased from Ossila and used as received. $FeCl_3$ was purchased from Sigma Aldrich. The solvents , 1,2-dichlorobenzene (purity > 99.9 %), Nitromethane (99.9%, extra dry, over molecular were purchased from Sigma Aldrich.

Thin film fabrication:

P3HT, PBTTT and OD-PDPP2T-TT powders were dissolved in dichlorobenzene (DCB) with 10mg/ml concentration and stirred overnight at 70 °C on hot plate. The polymer solutions were spin coated (1000 rpm for 90 s) on pre-cleaned (acetone, isopropanol and UV-Ozone cleaner) and pre-patterned quartz substrates for electrical and thermoelectric measurements. Pre-cleaned n-doped silicon substrates were used for GIWAX scattering measurement. For UV-Vis measurement, films were spun coated on pre-cleaned 1 inch quartz substrates. Sequential doping was performed in glove box (O_2 < 1ppm; H_2O < 1ppm) using 0.03 M of $FeCl_3$ solution in Nitromethane by dipping the polymer film in dopant solution for 5 second.

GIWAXS Measurement:

GIWAXS measurements were performed in Lawrence Berkeley national lab. The energy of the incident beam was at 10 keV, and a Pilatus 2 M area detector was used. The X-ray scattering data were taken at incidence angles of 0.14°∓0.005° with 1−5 s exposure times. The samples were kept under helium environment during X-ray exposure to minimize air scattering and sample degradation. Samples were doped before measurement. Before loading, samples resistance was measured. It was in ~1K Ohm range. After measurement, samples resistance was measured again, and it was found in ~2K Ohm range. Therefore, before and after measurement, the films were still heavily doped.

UV-Vis Measurement:

A Shimadzu UV 3600 spectrophotometer was used to measure absorption spectra of pristine and doped polymer samples. Quartz substrate was used as reference. The absorption was measured from 4 eV to down to 0.5 eV. The films were doped just before the absorption measurement to avoid any degradation issue.

FTIR Measurement:

A Bruker VERTEX 80v spectrophotometer was used to measure FTIR absorption spectra of doped polymer samples. KBr disc were used as substrate. The polymer films were spin coated on KBr disc. The absorption was measured from 0.9 eV to down to 0.1 eV. The films were doped just before the absorption measurement to avoid any degradation issue.

Electrical and Thermoelectric characterization:

Electrical conductivity and Seebeck coefficient of polymer thin films were measured using a shadow mask technique to pattern the heater and the electrodes to measure in the in-plane thermoelectric properties. Polymer film is spin-coated on a pre-patterned quartz substrate. After

sequential doping, the films were loaded in a high-vacuum (~10^{-6} torr) cryostat for electrical and thermoelectric measurements. The films thickness was measured before performing de-doping measurement with a KLA Tencor profilometer. The vacuum chamber with heating stage was used to de-dope the polymer films; the dopant slowly evaporates out of the film and de-dopes the film sequentially in time at room temperature. After reaching vacuum de-doping saturation at room temperature, the film was annealed in vacuum at 50°C for 30 min and then bring back to room temperature for measurement. This process was repeated multiple times to remove dopant further. The measurement was performed until sample resistance reaches in 1 MOhm range. Above 1Mohm, open circuit voltage was noisy and signal to noise ratio was higher. Electrical conductivity and Seebeck coefficient were calculated as a function of this de-doping.

Dielectric measurement:

Metal insulator semiconductor (MIS) device structure was used to measure low frequency dielectric constant of pristine polymer materials as shown in Fig. S4. P3HT, PBTTT and OD-PDPP2T-TT were dissolved in dichlorobenzene (DCB) with 10mg/ml concentration and stirred overnight at 70 °C on hot plate. The polymer solutions were then spun casted onto pre-cleaned SiO2(300 nm)/Si substrates at 1000 rpm in N_2 filled glove box. The spin coated films were annealed at 120 °C for 10 min to remove the solvent residue. Thickness of the films were measured using KLA Tencor profilometer. Thickness of 33 ± 5 nm were found for P3HT and PBTTT and 63± 5 nm for OD-PDPP2T-TT. 10 nm Cr and 100 nm Au were deposited as electrodes with different surface areas using a shadow mask. Device fabrication was performed in a N_2-filled glovebox. Keithley 4200 with CVU option was used to measure the capacitance of each area size device. An a.c. voltage of 100 m V and 10 KHz frequency and a d.c. voltage sweep from +30 V to -10V were applied for measurement. The capacitance of SiO_2 without polymer film was measured as a function of different electrode dot size. After that polymer films capacitance with different electrode do size was measured. +30 V was applied to structure to ensure a fully depleted device. The depleted polymer layer acts as a capacitor in series with the SiO_2 layer, and hence the total capacitance is:

$$\frac{1}{C_{exp}} = \frac{1}{C_{SiO_2}} + \frac{1}{C_{Polymer}} \quad (1)$$

where C_{SiO_2} and $C_{Polymer}$ are the capacitances of SiO_2 and the polymer, respectively. After extracting capacitance of polymer thin film, dielectric constant of polymer was calculated using following equation:

$$C_{Polymer} = \frac{\varepsilon_0 \varepsilon_r A}{t} \quad (2)$$

where A is the electrode area, ε_r the polymer dielectric constant, ε_0 the vacuum permittivity and *t* the polymer film thickness.

Acknowledgement:

P.K., and K.H. would like to acknowledge funding from the Materials Generative Design and Testing Framework (MAT-GDT) Program at A*STAR, provided through the AME Programmatic Fund (Grant No. M24N4b0034).

Supplementary Information:

Details about electrical characterization and theoretical calculation are available in SI.

References:

[1] Haddad, C.; Périlhon, C.; Danlos, A.; François, M.X.; Descombes, G. Some Efficient Solutions to Recover Low and Medium Waste Heat: Competitiveness of the Thermoacoustic Technology. *Energy Procedia* **2014**, *50*, 1056–1069.

[2] Shi, X. L.; Zou, J.; Chen, Z. G. Advanced Thermoelectric Design: From Materials and Structures to Devices. Chem. Rev. **2020**, 120 (15), 7399–7515.

[3] Snyder, G.; Toberer, E.; Complex Thermoelectric Materials. Nat. Mater. **2008**, 7, 105-114.

[4] Bubnova, O.; Khan, Z. U.; Malti, A.; Braun, S.; Fahlman M.; Berggren M.; Crispin X. Optimization of the Thermoelectric Figure of Merit in the Conducting Polymer Poly(3,4-Ethylenedioxythiophene), Nat. Mater. **2011**, 10(6), 429-433.

[5] Kim, G. H.; Shao, L.; Zhang, K.; Pipe, K. P. Engineered Doping of OrganicSemiconductors for Enhanced Thermoelectric Efficiency, Nat. Mater. **2013**, 12(8), 719-723.

[6] Bubnova, O.; Khan, Z. U.; Wang, H.; Braun, S.; Evans, D. R.; Fabretto, M.; Hojati-Talemi, P.; Dagnelund, D.; Arlin, J. B.; Geerts, Y. H.; Desbief, S.; Breiby, D. W.; Andreasen, J. W.; Lazzaroni, R.; Chen, W. M.; Zozoulenko, I.; Fahlman, M.; Murphy, P. J.; Berggren, M.; Crispin, X. Semi-metallic Polymers. Nat. Mater. **2014**, 13(2), 190-194.

[7] Vijayakumar, V.; Zhong, Y.; Untilova, V.; Bahri, M.; Herrmann, L.; Biniek, L.; Leclerc, N.; Brinkmann, M. Bringing Conducting Polymers to High Order: Toward Conductivities beyond 10^5 S cm^{-1} and Thermoelectric Power Factors of 2 mW m^{-1} K^{-2}. Adv. Ener. Mater. **2019**, 9(24), 1900266.

[8] Untilova, V.; Hynynen, J.; Hofmann, A. I.; Scheunemann, D.; Zhang, Y.; Barlow, S.; Kemerink, M.; Marder, S. R.; Biniek, L.; Müller, C.; Brinkmann, M. High Thermoelectric Power Factor of Poly(3-hexylthiophene) through In-Plane Alignment and Doping with a Molybdenum Dithiolene Complex. *Macromol.* **2020,** 53(15), 6314-6321.

[9] Glaudell, A. M.; Cochran, J. E.; Patel, S. N.; Chabinyc, M. L. Impact of the Doping Method on Conductivity and Thermopower in Semiconducting Polythiophenes. *Adv. Ener. Mater.* **2015**, 5, 1401072.

[10] Lim, E.; Peterson, K. A.; Su, G. M.; Chabinyc, M. L. Thermoelectric Properties of Poly(3-hexylthiophene) (P3HT) Doped with 2,3,5,6-Tetrafluoro-7,7,8,8-tetracyanoquinodimethane (F4TCNQ) by Vapor-Phase Infiltration. *Chem. Mater.* **2018**, 30(3), 998-1010.

[11] Patel S. N.; Glaudell A. M.; Peterson K. A.; Thomas E. M.; O'Hara K. A.; Lim E.; Chabinyc M. L. Morphology Controls the Thermoelectric Power Factor of a Doped Semiconducting Polymer *Sci. Adv.* **2017**, 3, e1700434.

[12] Rivnay, J.; Vandewal, K.; Koch, F. P. V.; Stingelin, N.; Smith, P.; Toney, M. F.; Salleo. A General Relationship Between Disorder, Aggregation and Charge Transport in Conjugated Polymers. *Nat. Mater.* **2013**, 12(11), 1038-1044.

[13] Jacobs, I. E.; Aasen, E. W.; Oliveira, J. L.; Fonseca, T. N.;Roehling, J. D.; Li, J.; Zhang, G.; Augustine, M. P.; Mascal, M.;Moule, A. J. Comparison of Solution-Mixed and Sequentiallý Processed P3HT:F4TCNQ Films: Effect of Doping-InducedAggregation on Film Morphology. J. Mater. Chem. C **2016,**4,3454−3466.

[14] Scholes, D. T.; Hawks, S. A.; Yee, P. Y.; Wu, H.; Lindemuth, J. R.; Tolbert, S. H.; Schwartz, B. J. Overcoming Film Quality Issues for Conjugated Polymers Doped with F_4TCNQ by Solution Sequential Processing: Hall Effect, Structural, and Optical Measurements. *J. Phy. Chem. Lett.* **2015,** 6(23), 4786-4793.

[15] Scholes, D. T.; Yee, P. Y.; Lindemuth, J. R.; Kang, H.; Onorato,. J.; Ghosh, R.; Luscombe, C. K.; Spano, F. C.; Tolbert, S. H.; Schwartz, B. J. The Effects of Crystallinity on Charge Transport and theStructure of Sequentially Processed F4TCNQ-Doped ConjugatedPolymer Films. Adv. Funct. Mater.**2017**,27(44), 1702654.

[16] Vijayakumar, V.; Durand, P.; Zeng, H.; Untilova, V.; Herrmann, L.; Algayer, P.;. Leclerc, N. and Brinkmann, M. Influence of Dopant Size and Doping Method on the Structure and Thermoelectric Properties of PBTTT Films Doped with F_6TCNNQ and F_4TCNQ. *J. Mater. Chem. C* **2020**, 8, 16470-16482.

[17] Aubry, T. J.; Winchell, K. J.; Salamat, C. Z.; Basile, V. M.; Lindemuth, J. R.; Stauber, J. M.; Axtell, J. C.; Kubena, R. M.; Phan, M. D.; Bird, M. J.; Spokoyny, A. M.; Tolbert, S. H.; Schwartz, B. J. Tunable Dopants with Intrinsic Counterion Separation Reveal the Effects of Electron Affinity on Dopant Intercalation and Free Carrier

Production in Sequentially Doped Conjugated Polymer Films. *Adv. Func. Mater.* **2020**, 30, 2001800.

[18] Brebels, J.; Manca, J. V.; Lutsen, L.; Vanderzande, D.; Maes, W.High Dielectric Constant Conjugated Materials for Organic Photo-voltaics. J. Mater. Chem. A **2017**, 5, 24037−24050.

[19] Cho, N.; Schlenker, C. W.; Knesting, K. M.; Koelsch, P.; Yip, H.-L.; Ginger, D. S.; Jen, A. K.-Y. High-Dielectric Constant Side-Chain Polymers Show Reduced Non-Geminate Recombination in Heterojunction Solar Cells. Adv. Energy Mater. **2014**, 4 (10), 1301857.

[20] Brebels, J.; Douvogianni, E.; Devisscher, D.; Eachambadi,, R.T.; Manca, J.; Lutsen, L.; Vanderzande, D.; Hummelen, J.C.; Maes, W. An Effective Strategy to Enhance the Dielectric Constant of Organic Semiconductors-CPDTTPD-based Low Bandgap Polymers Bearing oligo(ethylene glycol) side chain. J. Mater. Chem. C, **2018**, 6, 500-511.

[21] Wang, C.; Zhang, Z.; Pejić, S.; Li, R.; Fukuto, M.; Zhu, L.; Sauvé, G. High Dielectric Constant Semiconducting Poly(3-alkylthiophene)s from Side Chain Modification with Polar Sulfinyl and Sulfonyl Groups. *Macromol.* **2018**, 51(22), 9368-9381.

[22] Marszalek, T.; Li, M.; Pisula, W. Design Directed Self-assembly of Donor–acceptor Polymers. *Chem. Comm.* **2016**, 52, 10938-10947.

[23] Yiu, A. T.; Beaujuge, P. M.; Lee, O. P.; Woo, C. H.; Toney, M. F.; Fréchet, J. M. J. Side-Chain Tunability of Furan-Containing Low-Band-Gap Polymers Provides Control of Structural Order in Efficient Solar Cells. *J. Am. Chem. Soc.* **2012**, 134(4) ,2180-2185.

[24] Zhang, G.; Clarke, T. M.; Mozer, A. J. Bimolecular Recombination in a Low Bandgap Polymer:PCBM Blend Solar Cell with a High Dielectric Constant. *J. Phy. Chem. C* **2016**, 120(13), 7033-7043.

[25] Sirringhaus, H.; Brown, P. J.; Friend, R. H.; Nielsen, M. M.;Bechgaard, K.; Langeveld-Voss, B. M. W.; Spiering, A. J. H.;Janssen, R. A. J.; Meijer, E. W.; Herwig, P.; de Leeuw, D. M. Two-dimensional Charge Transport in Self-organized, High-mobility Conjugated Polymers. *Nat.* **1999**, 401, 685-688.

[26] McCulloch, I.; Heeney, M.; Bailey, C.; Genevicius, K.; Macdonald, I.; Shkunov, M.; Sparrowe, D.; Tierney, S.; Wagner, R.; Zhang, W.; Chabinyc, M.L.; Kline, R.J.; Mcgehee M.D.; Toney, M.F. Liquid-CrystallineSemiconducting Polymers with High Charge-Carrier Mobility, Nat. Mater. **2006** 5(4), 328-333.

[27] Zhang, X.; Richter, L. J.; DeLongchamp, D. M.; Kline, R. J.; Hammond, M. R.; McCulloch, I.; Heeney, M.; Ashraf, R. S.; Smith, J. N.; Anthopoulos, T. D.; Schroeder, B.; Geerts, Y. H.; Fischer, D. A.; Toney, M. F. Molecular Packing of High-Mobility Diketo

Pryyolo-Pyrrole Polymer Semiconductors with Branched Alkyl Side Chains. *J.Am. Chem. Soc.* **2011**, 133, 15073.

[28] Rivnay, J.; Noriega, R.; Kline, R. J.; Salleo A.; Toney M. F. Quantitative Analysis of Lattice Disorder and Crystallite Size in Organic Semiconductor Thin Films. *Phy. Rev. B* **2011**, 84, 045203.

[29] Tanaka, H.; Kanahashi, K.; Takekoshi, N.; Mada, H.; Ito, H.; Shimoi, Y.; Ohta, H.; Takenobu, T. Thermoelectric Properties of a Semicrystalline Polymer Doped Beyond the Insulator-to-Metal Transition by Electrolyte Gating. *Sci. Adv.* **2020**, 6, eaay8065.

[30] Ghosh, R.; Pochas, C. M.; Spano, F. C. Polaron Delocalization in Conjugated Polymer Films. *J. Phy. Chem. C* **2016**, 120(21), 11394-11406.

[31] Rasmussen, S. C.; Straw, B. D.; Hutchison J.E. Tuning the Extent of Conjugation in Processable Polythiophenes Through Control of Side Chain Density and Regioregularity. "Semiconducting Polymers",**1999**, *ACS Symposium Series* Vol. 735, Chapter 21, pp347-366.

[32] Salleo, A.; Kline, R.J.; DeLongchamp, D. M. ; Chabinyc, M. L. Microstructural Characterization and Charge Transport in Thin Films of Conjugated Polymers. *Adv. Mater.* **2010**, 22(34), 3812-3838.

[33] Cochran, J. E.; Junk, M. J. N.; Glaudell, A. M.; Miller, P. L.;. Cowart, J. S.; Toney, M. F.; Hawker, C. J.; Chmelka, B. F.;. Chabinyc, M. L. Molecular Interactions and Ordering in Electrically Doped Polymers: Blends of PBTTT and F4TCNQ. *Macromol.* **2014**, 47 6836.

[34] Jacobs, I.E.; Lin, Y.; Huang, Y.; Ren, X.; Simatos, D.; Chen, C.; The, D.; Statz, M.; Lai, L.; Finn, P. A.; Neal, W. G.; D'Avino, G.; Lemaur, V.; Fratini, S.; Beljonne, D.; Strzalka, J.; Nielsen, C. B.; Barlow, S.; Marder, S. R.; McCulloch I.; Sirringhaus, H. High-Efficiency Ion-Exchange Doping of Conducting Polymers. Adv. Mater. **2022**, 34, 2102988.

[35] Aubry T. J.; Axtell J. C.; Basile V. M.; Winchell K. J.; Lindemuth J. R.; Porter T. M.; Liu J. Y.; Alexandrova A. N.; Kubiak C. P.; Tolbert S. H.; Spokoyny A. M.; Schwartz B. J. Dodecaborane-Based Dopants Designed to Shield Anion Electrostatics Lead to Increased Carrier Mobility in a Doped Conjugated Polymer. Adv. Mater. **2019**, 31, 1805647.

[36] Thomas, E. M.; Peterson, K. A.; Balzer, H.; Rawlings, D.; Stingelin, N.; Segalman, R. A.; Chabinyc, M. L. Effects of Counter-Ion Size on Delocalization of Carriers and Stability of Doped Semiconducting Polymers Adv. Electron. Mater. **2020**, 6, 2000595.

[37] Lim, S. W.; Shimogaki, Y.; Nakano, Y.; Tada, K.; Komiyama, H. Preparation of Low-Dielectric-Constant F-Doped SiO_2 Films by Plasma-Enhanced Chemical Vapor Deposition Jap. J. Appl. Phys. **1996**, 35, 1468.

[38] Abutaha, A.; Kumar, P.; Yildirim, E.; Shi, W.; Yang, S. W.; Wu, G.; Hippalgaonkar, K. Correlating Charge and Thermoelectric Transport to Paracrystallinity in Conducting Polymers. Nat. Comm. **2020**, 11, 1737.

[39] Guangzheng, Z.; Abdalla, H.; Kemerink, M. Impact of doping on the density of states and the mobility in organic semiconductors. Phy. Rev. **2016**, 93, 235203.

[40] Abdalla, H.; Guangzheng, Z.; Kemerink, M. Range and energetics of charge hopping in organic semiconductors. Phy. Rev. **2017**, 96, 241202(R).

TOC Figure: